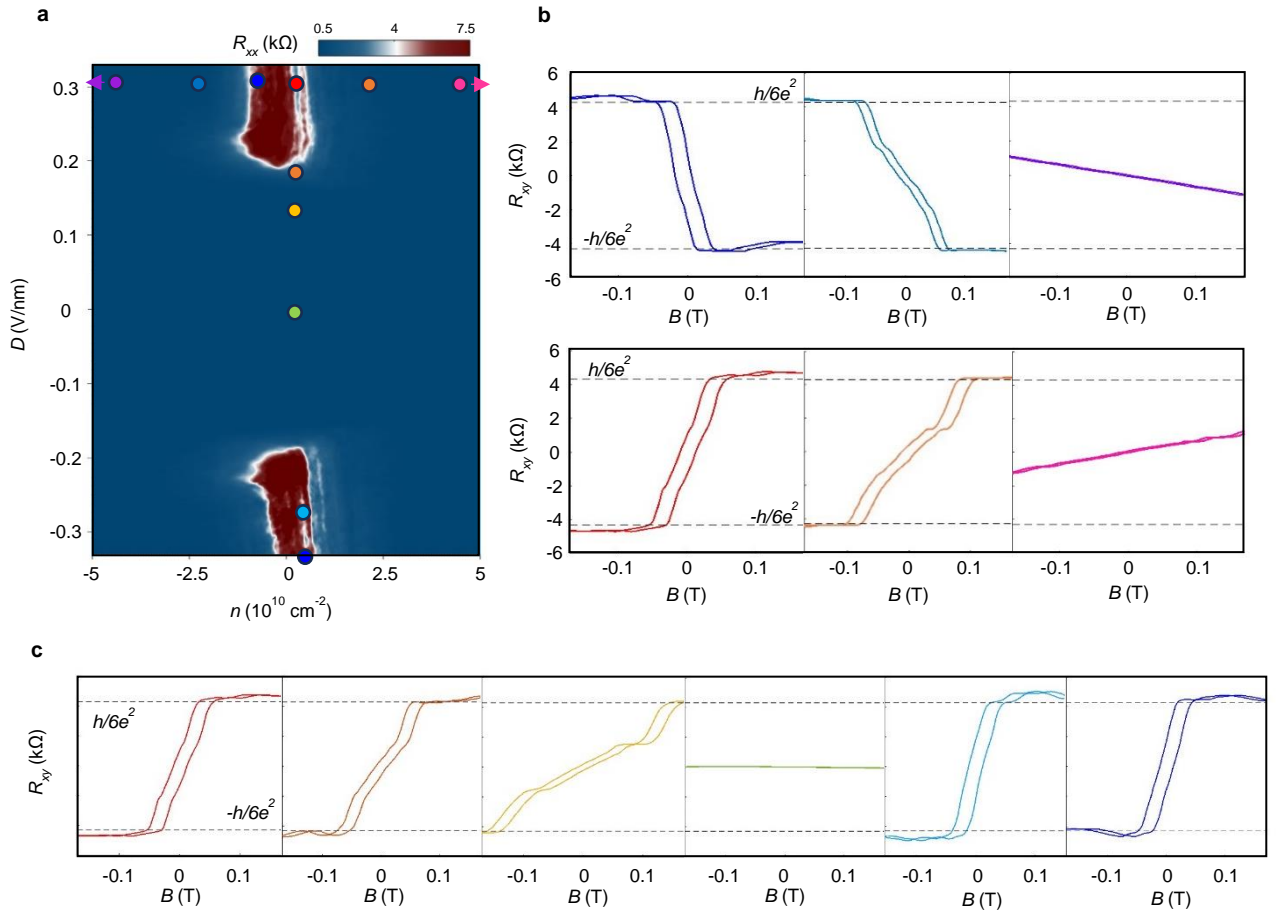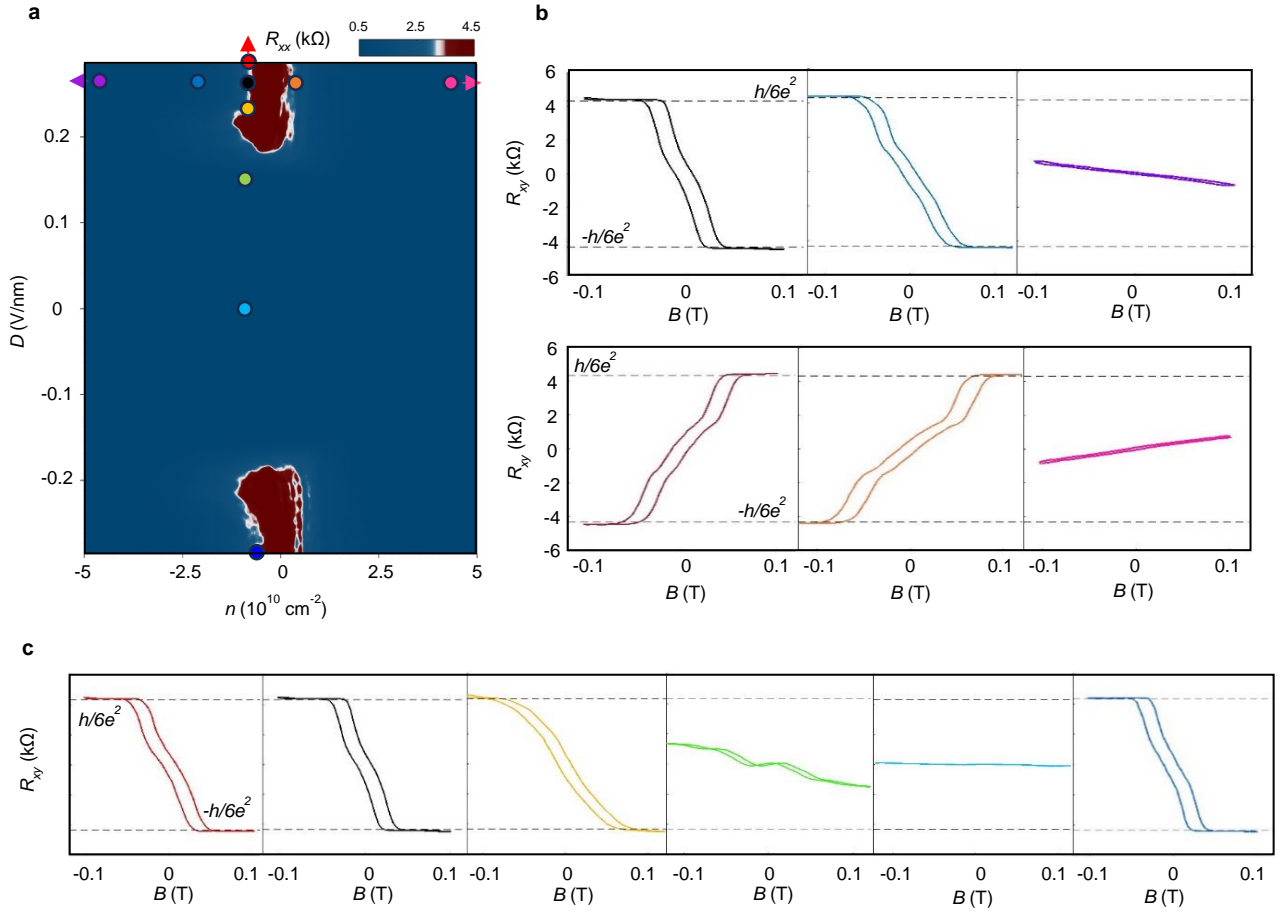Extended Data Fig.1 Optical images of the devices.a, c, e, Optical images of final stack of the BTG devices D1 (a), D2 (c) and D3 (e). Dashed lines show the lines along the Bernal tetralayer graphene and hBN flakes edge. The black line represents the edge of the BTG, the white and pink lines represent the edges of the bottom and top hBN, respectively. In device D1, the angle between the BTG and the bottom hBN is 14 degrees, while in device D2 and device D3, the angle between the BTG and the bottom hBN is 10 degrees. **b, d, f,** Optical images of completed BTG devices D1 (b), D2 (d) and D3 (f). All scale bars, 10 μm.
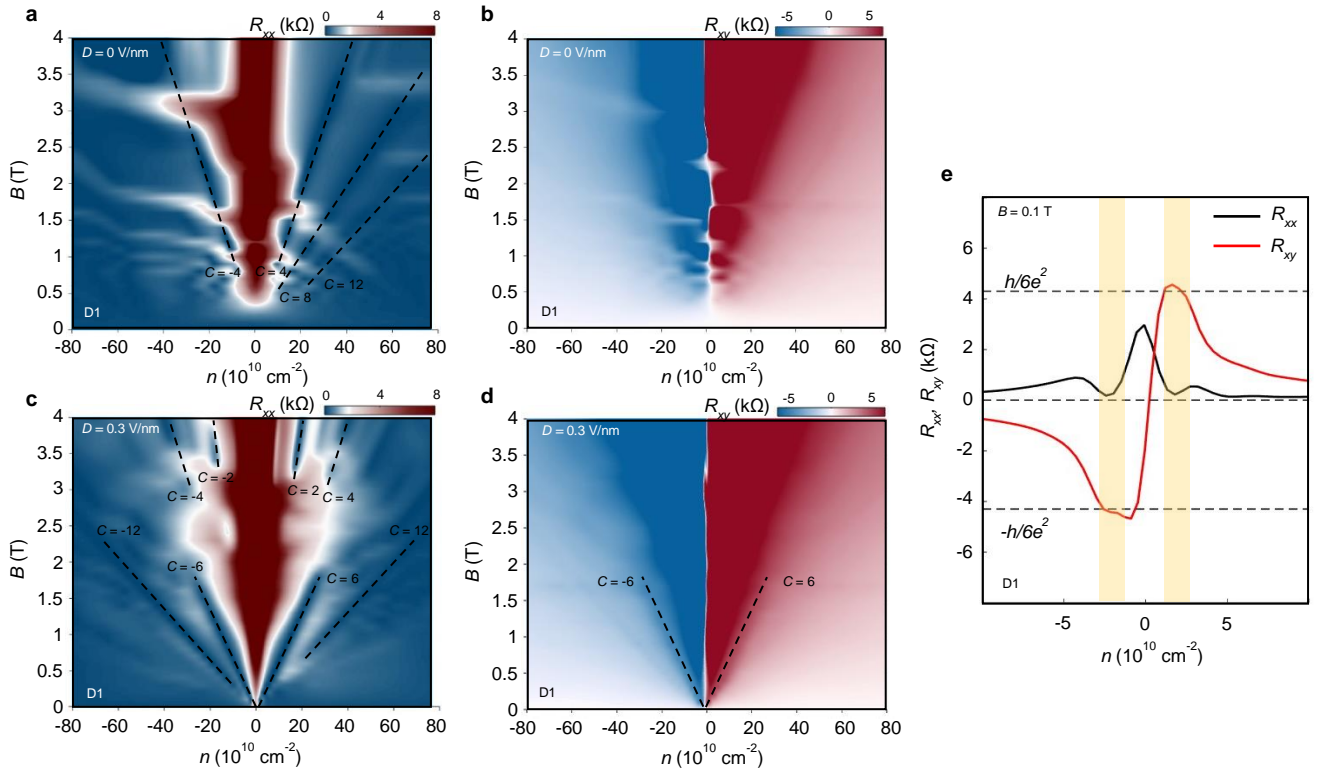
Extended Data Fig.2 Development of R_{xy} hysteresis loops at different (n, D) condition in device D1.
a, R_{xx} $n - D$ phase diagram at $B = 0$ T. **b,** Magnetic hysteresis loops of R_{xy} under varying carrier density n with fixed displacement field $D = 0.3$ V/nm. The (n, D) conditions are denoted by color of dots in **a**. **c,** Magnetic hysteresis loops of R_{xy} under varying displacement field D with fixed carrier density $n = 1.0 \times 10^{10}$ cm^{-2}. The (n, D) conditions are denoted by color of dots in **a**.

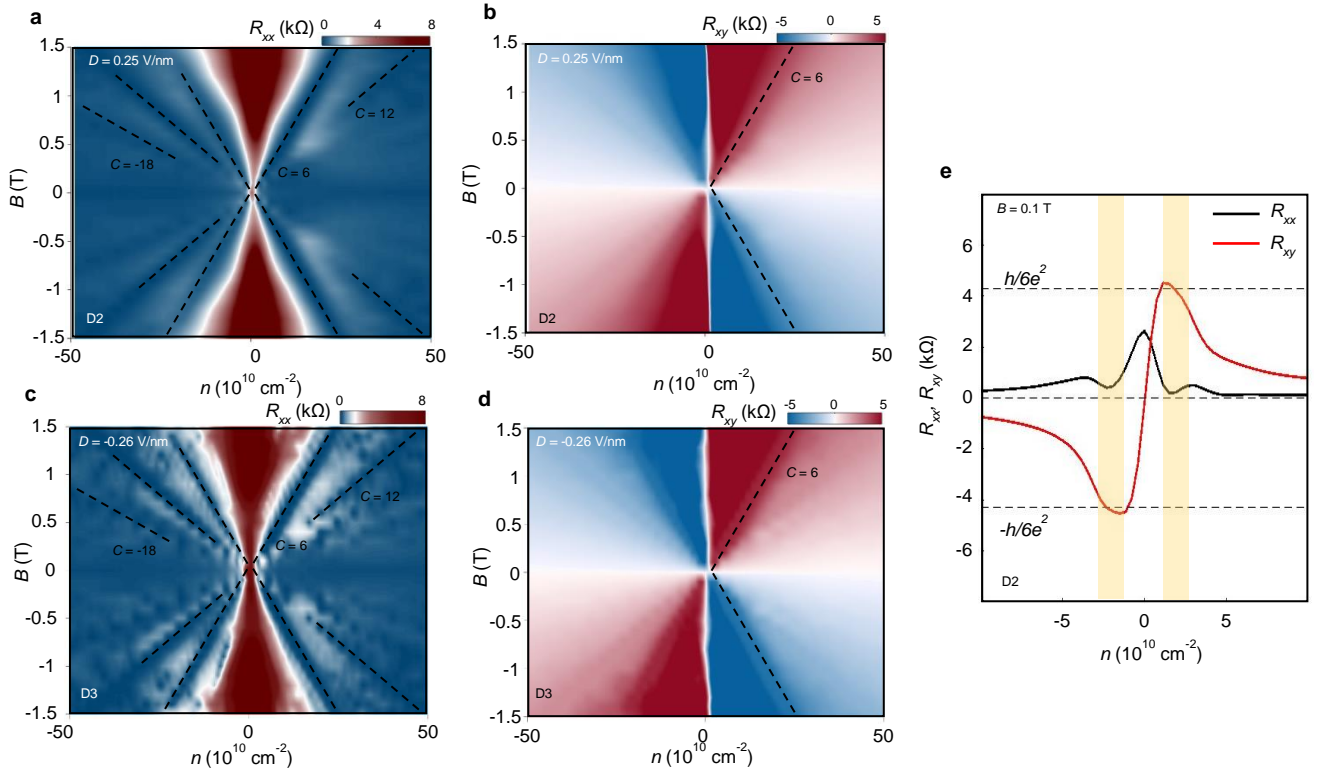**Extended Data Fig.3 Development of R_{xy} hysteresis loops at different (n, D) condition in device D2. a,** R_{xx} $n - D$ phase diagram at $B = 0$ T. **b,** Magnetic hysteresis loops of R_{xy} under varying carrier density n with fixed displacement field $D = 0.25$ V/nm. The (n, D) conditions are denoted by color of dots in **a**. **c,** Magnetic hysteresis loops of R_{xy} under varying displacement field D with fixed carrier density $n = -1.0 \times 10^{10}$ cm^{-2}. The (n, D) conditions are denoted by color of dots in **a**.
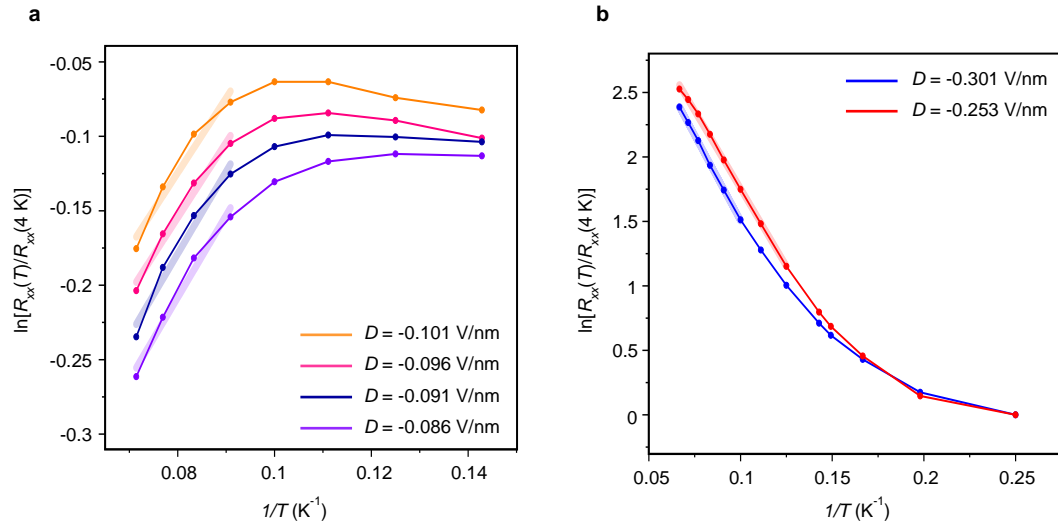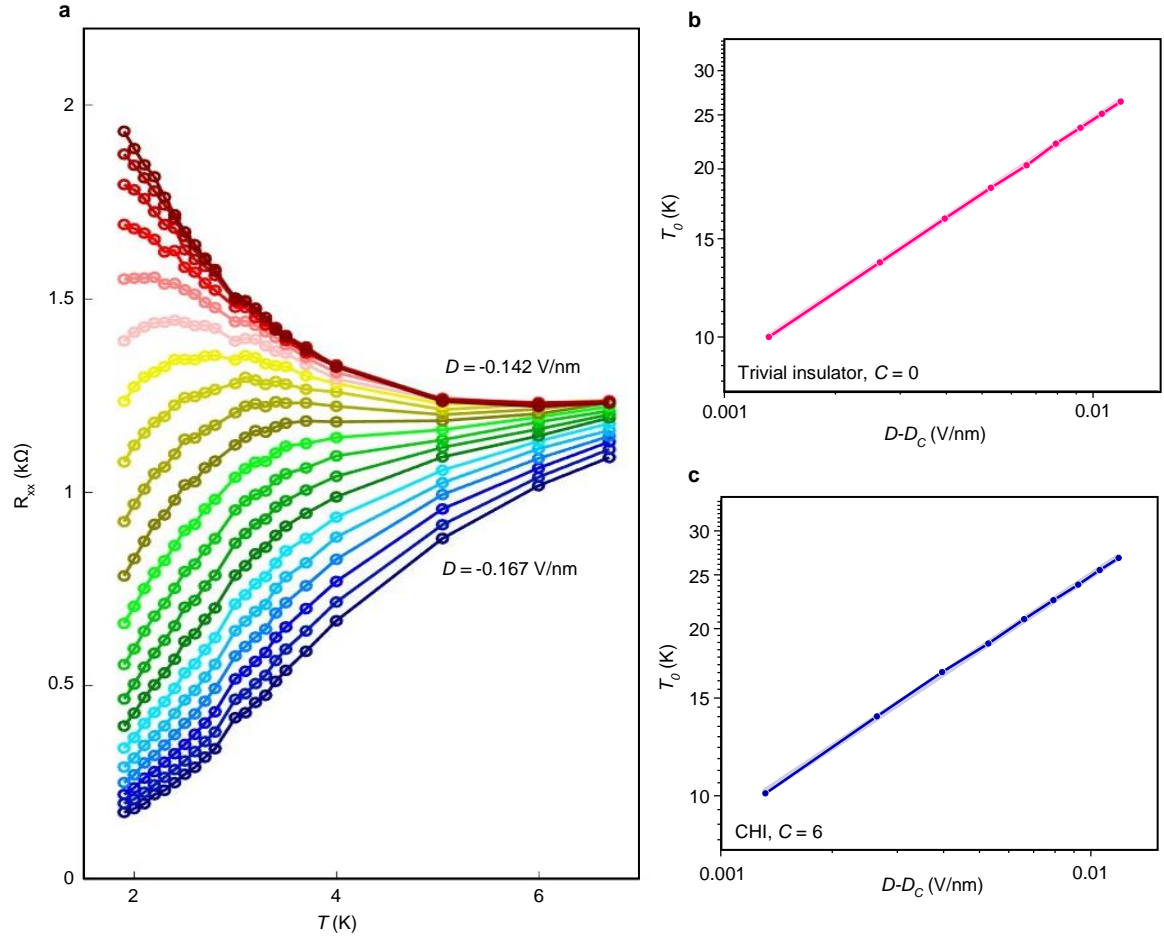
Extended Data Fig.4 Landau fan diagram depending on the displacement field in device D1. a, b, Landau fan diagrams of R_{xx} (a) and R_{xy} (b) at $D = 0\,\text{V/nm}$, $T = 3\,\text{K}$. CHI phase does not appear at low displacement field. **c, d,** Landau fan diagrams of R_{xx} (c) and R_{xy} (d) at $D = 0.3\,\text{V/nm}$, $T = 3\,\text{K}$. $C = 6$ CHI phase appears at $D = 0.3\,\text{V/nm}$. $C = \pm 6$ Streda slopes exist below $B = 0.4\,\text{T}$. **e,** R_{xx}(black) and R_{xy}(red) measured as a function of n at $B = 0.1\,\text{T}$, $D = 0.3\,\text{V/nm}$, $T = 3\,\text{K}$. R_{xx} is close to zero at the carrier density where the R_{xy} is well quantized at $h/6e^2$, indicating a Chern insulator with $C = 6$.
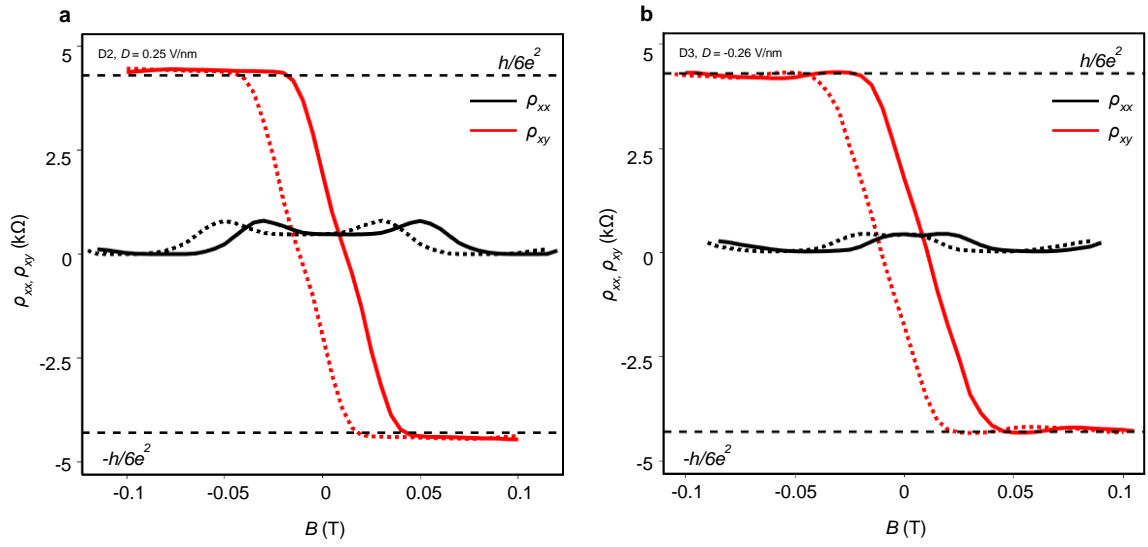
Extended Data Fig.5 Landau fan diagram in device D2 and device D3. a, b, Landau fan diagrams of R_{xx} (a) and R_{xy} (b) at $D = 0.25$ V/nm, $T = 3$ K in device D2. $C = 6$ CHI phase appears at $D = 0.25$ V/nm. $C = \pm6$ Streda slopes exist below $B = 0.4$ T. **c, d,** Landau fan diagrams of R_{xx} (c) and R_{xy} (d) at $D = -0.26$ V/nm, $T = 10$ mK in device D3. $C = 6$ CHI phase appears at $D = -0.26$ V/nm. $C = \pm6$ Streda slopes exist below $B = 0.3$ T. **e,** R_{xx}(black) and R_{xy}(red) measured as a function of n at $B = 0.1$ T, $D = 0.25$ V/nm, $T = 3$ K in device D2. R_{xx} is close to zero at the carrier density where the R_{xy} is well quantized at $h/6e^2$, indicating a Chern insulator with $C = 6$. The CHI phase is highly reproducible upon repeated measurements, even in device D2 and device D3.

Extended Data Fig.6 Extraction of thermal activation gap in Device D1. a, b, Arrhenius plot of $R_{xx}(T)$ at various D. $R_{xx}(T)$ value is normalized by its value at $T = 4$ K. The highlighted lines are fits to the thermal activation behavior from trivial insulator state(a) and CHI state(b).

Extended Data Fig.7 Quantum critical scaling analysis in Device D1. a, R_{xx} measured as a function of T at $B = 80$ mT under varying displacement fields. **b, c,** $|D - D_C|$ versus T_0 curve in scaling analysis for trivial insulator state (b) and C=6 CHI state (c). The highlighted lines are fits to the power-law behaviors: $T_0 = |D - D_c|^{zv}$, with $zv = 0.44 \pm 0.002$.

Extended Data Fig.8 Hall angle at zero magnetic field in device D2 and device D3. a, b, Symmetrization of ρ_{xx} (black) and anti-symmetrization of ρ_{xy} (red) measured as a function of B at $n = -1.3 \times 10^{10}$ cm^{-2}, $T = 10$ mK in device D2 (a) and device D3 (b). ρ_{xy}/ρ_{xx} exhibits a large value exceeding 2.0, indicating a large anomalous Hall angle.